All-optical multichannel 2R regeneration in a fiber-based device

Michael Vasilyev

Department of Electrical Engineering, University of Texas at Arlington, Arlington, Texas 76019-0016

Taras I. Lakoba

Department of Mathematics and Statistics, University of Vermont, Burlington, Vermont 05405

Received October 1, 2004

We propose the design of an all-optical 2R regenerator capable of handling multiple wavelength-division-multiplexed channels simultaneously. It extends the known concept of off-center filtering of self-phase-modulation-broadened signal spectra. The novel feature of the proposed device is a dispersion map that strongly suppresses interchannel impairments. The map employs several sections of nonlinear fiber with high normal dispersion, separated by dispersion compensators with spectrally periodic group delay. The results of our numerical simulations indicate the feasibility of such a multichannel regenerator. © 2005 Optical Society of America

OCIS codes: 060.4370, 060.5530, 060.2330.

All-optical regeneration has been recognized as a potential enabler of future ultralong-reach high-bit-rate systems and all-optical packet-switched networks. The fiber-based regenerator with a 2R (reamplification and reshaping) capability proposed in Ref. 1 has attracted particular attention because of its simplicity and robustness. This device is based on off-center optical bandpass filtering of the signal spectrum broadened by self-phase modulation (SPM) in a piece of highly nonlinear fiber (HNLF) with normal (nonsoliton) dispersion. Such a regenerator is able to improve the quality of both ZERO and ONE symbols, as has been demonstrated experimentally[1–3] and analyzed numerically.[4] To qualify itself as a viable alternative to state-of-the-art electronic-domain regenerators, an all-optical regenerator must be scalable with the number of wavelength-division-multiplexing (WDM) channels. However, simultaneous multichannel regeneration remains a formidable challenge because the operation of an all-optical regenerator fundamentally relies on strong nonlinear optical effects leading to debilitating interaction among the WDM channels. For example, in a recent study,[5] in a regenerator based on soliton filtering, interchannel four-wave mixing (FWM) was successfully suppressed, but strong cross-phase modulation (XPM) forced the use of polarization interleaving and limited the total number of regenerated channels to four.

In this Letter we propose a novel design of an all-optical 2R regenerator capable of simultaneous regeneration of multiple WDM channels and support this concept with numerical simulations. Our design allows one to suppress both the FWM and the XPM without the need for any polarization control. The proposed regenerator consists of multiple HNLF sections with high normal dispersion, separated by dispersion-compensating periodic-group-delay devices (PGDDs) [see Fig. 1(a)]. At the output of the regenerator, a spectrally periodic, optical bandpass filter (OBPF) selects off-center spectral regions of multiple WDM channels, similarly to the single-channel case.[1] To leave just enough space for the SPM-broadened spectra, we use a standard 1:4 deinterleaver[6] at the regenerator input, which separates the incoming WDM channels into four sets with four times greater channel spacing. The essential feature of the proposed regenerator is the dispersion map, which strongly suppresses nonlinear interchannel interactions (FWM and XPM) by means of high (normal) dispersion accumulated between the channels. At the same time, it keeps the dispersive walk-off among different spectral components of the same channel low to provide sufficient SPM-induced spectral broadening while preserving the integrity of the pulses. The key component of the above dispersion map is the PGDD, whose spectrally periodic group delay [Fig. 1(b)] ensures fast bit walk-off between the

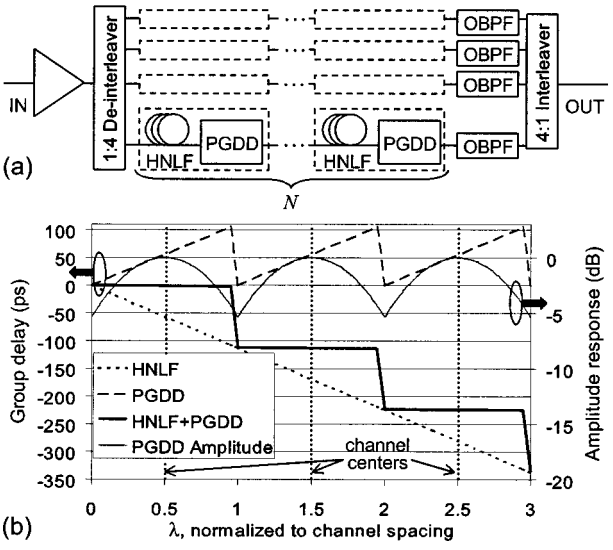

Fig. 1. (a) Schematic of the proposed multichannel dispersion-managed regenerator. In simulations reported in this study, $N=16$. (b) Group delay of the HNLF (dotted line), PGDD (dashed curve), and a single HNLF PGDD cell (thick solid curve). Thin solid curve, amplitude transfer function of the PGDD (not considered in 10-Gbit/s simulations).

0146-9592/05/121458-3/$15.00

neighboring channels and thereby suppresses the interchannel XPM. This feature of PGDD was recently used in a different application, where it greatly enhanced the quality of dispersion-managed-soliton transmission.[7,8] Let us note that the multiple PGDDs do not significantly contribute to the physical dimensions of the regenerator because they can be integrated by use of silica-on-silicon technology.[9,10]

The evolution equation inside a dispersion-managed regenerator has the following nondimensional form:

$$iu_{\xi}+\frac{1}{2}[S_{\mathrm{av}}+\tilde{S}(\xi)]u_{\tau\tau}+G(\xi)u|u|^2=0. \qquad (1)$$

Here $\xi=z/L_{\mathrm{map}}$, where z is the propagation distance and $L_{\mathrm{map}}=L_1+L_2$ is the length of one cell [dashed boxes in Fig. 1(a)] of the regenerator, with L_1 and L_2 being the lengths of the HNLF and the dispersion-compensating module (DCM), respectively. In the simulations reported below the DCM is taken as either a PGDD or a conventional fiber-based device. Nondimensional electric field u is normalized so that $P_0|u|^2$ is the signal power, where P_0 is the input peak power of the pulse. The time is normalized to input pulse width T: $t=\tau T$. [Here and below we quote the temporal and spectral widths as full width at half-maximum (FWHM).] Nondimensional parameters S_{av} and $\tilde{S}$ characterize the average dispersion $D_{\mathrm{av}}=(D_1L_1+D_2L_2)/L_{\mathrm{map}}$ and the map strength, respectively:

$$S_{\mathrm{av}}=D_{\mathrm{av}}\kappa, \qquad (2a)$$

$$\tilde{S}(\xi)=\begin{cases}(D_1-D_{\mathrm{av}})\kappa, & 0<\xi<L_1/L_{\mathrm{map}}\\ (D_2-D_{\mathrm{av}})\kappa, & L_1/L_{\mathrm{map}}<\xi<1\end{cases}. \qquad (2b)$$

Here D_1 and D_2 are chromatic dispersions of the HNLF and the DCM, $\kappa=L_{\mathrm{map}}\lambda^2/(2\pi cT^2)$, λ is the carrier wavelength, and c is the speed of light. Function $\tilde{S}(\xi)$ is extended periodically for $1<\xi\leqslant N$, where N is the number of HNLF DCM cells in the regenerator [see Fig. 1(a)]. In the proof-of-principle simulations reported below, we assume that both the HNLF and the DCM are lossless and, moreover, that the DCM is linear and $L_2\ll L_1$ (hence $L_{\mathrm{map}}\approx L_1$). Then $G(\xi)=\gamma(\xi)P_0L_{\mathrm{map}}$, where the nonlinear coefficient $\gamma(\xi)=\gamma_1$ in the HNFL and $\gamma(\xi)=0$ in the DCM. The output of the regenerator is determined by the following parameters: $\xi_{\mathrm{max}}=N$; S_{av}; $S_1\approx\kappa D_1$; $G_1\approx\gamma_1P_0L_1$; the duty ratio; $\Delta\Omega_{\mathrm{OBPF}}=\Delta\omega_{\mathrm{OBPF}}T$, where $\Delta\omega_{\mathrm{OBPF}}$ is the offset of the OBPF's passband from the channel center; and $\Delta\Omega=\Delta\omega T$, where $\Delta\omega$ is the channel spacing. We note that losses of real HNLF and DCM can be dealt with by use of amplifiers or progressively smaller D_1 and larger L_1, so as to preserve S_1 and G_1.

Figure 2 shows the results of simulating Eq. (1) with one and five 10 Gbit/s channels spaced 200 GHz apart and each carrying a 2^7-1 pseudorandom bit sequence of 33 ps, chirp-free Gaussian pulses. All the channels are copolarized, and their pseudorandom bit sequence patterns are decorrelated. To reproduce the input pulse width at the output of the regenerator, the OBPF is taken as a 13.3 GHz Gaussian; it is offset by 25 GHz from the channel center. The (dispersionless) filters at the output of the transmitter (mux) and the input of the deinterleaver (demux) in Fig. 1(a) are third-order Gaussians with a FWHM of 35 GHz; they are wide enough not to cause any noticeable distortion to the pulses. We model the degradation of ones by 60% peak-to-peak amplitude jitter and that of zeros by a low 8 dB extinction ratio, as shown in Fig. 2(a). Their average peak power is 90 mW. Because our focus is on nonlinear effects, we do not simulate the amplified spontaneous emission noise. Each HNLF section of the regenerator has $\gamma_1=9\ \mathrm{W^{-1}\,km^{-1}}$, $D_1=-100$ ps/nm/km, $L_1=0.7$ km; the average dispersion is $D_{\mathrm{av}}=-1$ ps/nm/km, and we use 16 such sections [$N=16$ in Fig. 1(a)], so that the total length of the HNLF is 11.2 km. Figure 2(b) shows the optical eye of the output of the regenerator with the single-channel input. The other plots in Fig. 2 show the worst output channels of the five-channel input when the regenerator uses a fiber-based DCM [Fig. 2(c)] and a PGDD [Fig. 2(d)], both having the same chromatic dispersions near the channels' centers. We quantify the improvement of the signal quality in Fig. 2(d) compared with that in Fig. 2(a) by the eye opening within the 10 ps (i.e., 10% of the bit) window around the eye's maximum. For this comparison we rescale the amplitude of the output signal to make the average powers of the input and output equal to each other. The corresponding eye-opening improvement is 1.2 dB. Comparison of Figs. 2(c) and 2(d) proves that the PGDD is a key component of the proposed regenerator.

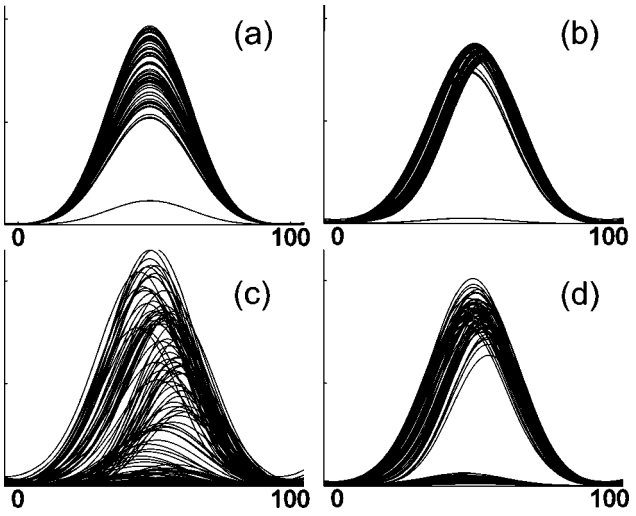

Fig. 2. Optical eye diagrams of the (a) input, (b) output of the single simulated channel, and (c),(d) worst-channel outputs for the five-channel input to the regenerator at 10 Gbits/s. The DCM is (c) fiber and (d) PGDD based.

We now show that the proposed multichannel regenerator, with one modification, can also improve 40 Gbit/s signals. We emphasize that this case does *not* reduce to a simple rescaling of the 10 Gbit/s case. This is because the spectral efficiency (the bit rate divided by the channel spacing) of 40 Gbit/s transmission systems proposed for commercial use is twice as

high as that of 10 Gbit/s systems: 0.4 versus 0.2. Specifically, the channel spacings are 100 and 50 GHz for the 40 and 10 Gbit/s systems, respectively. The increase in the spectral efficiency gives rise to two aspects in which 40 Gbit/s signals differ from their 10 Gbit/s counterparts: (i) the nondimensional channel spacing is smaller, and (ii) the pulses' duty ratio is higher for the 40 Gbit/s signals. Below we explain these statements and their consequences for the multichannel regeneration in more detail.

The mux and demux filters, defined earlier in the text, must have bandwidths narrower than the channel spacing. For 100 GHz spaced 40 Gbit/s channels we assume that they are both 85 GHz third-order Gaussians. Gaussian pulses having a width of 8.3 ps (i.e., 33% of the bit) get broadened by those filters to approximately 12 ps and therefore strongly overlap with one another. This strong overlap produces substantial distortions of the output of the regenerator even in the single-channel case.[11] To eliminate this overlap, we used carrier-suppressed return-to-zero (CSRZ) pulses, for which the field in any two adjacent bits has a phase shift of π. After passing through the mux–demux pair, CSRZ pulses broaden to approximately 13.5 ps, but their key advantage over the filtered Gaussian pulses is that the field between any two adjacent pulses passes through a zero. Therefore the filtered CSRZ pulses are more distinctly separated in a bit sequence than the filtered Gaussian pulses. However, even this improved pulse separation is not as good as that between 33% Gaussian pulses at 10 Gbits/s. As a consequence, the optimal map strength, $S_1 \approx \kappa D_1$, must be smaller for the 40 Gbit/s case in order not to result in adjacent pulse interaction. This is the first significant difference between the 40 and 10 Gbit/s cases.

The second difference is that the nondimensional channel spacing, $\Delta\Omega_{40G}=400\ \mathrm{GHz}\times 13.5\ \mathrm{ps}=5.4$ for 40 Gbits/s is less than that, $\Delta\Omega_{10G}=200\ \mathrm{GHz}\times 33\ \mathrm{ps}=6.6$, for 10 Gbits/s. (We used the FWHMs as the normalization factors, even though the shapes of the Gaussian and filtered CSRZ pulses are not the same.) The decreased $\Delta\Omega$ at 40 Gbits/s results in a signal distortion that comes from the PGDD. Namely, when the edge of the signal spectrum broadened by the HNLF reaches the frequency located midway between two channels, the spectral components of the edge undergo strong distortions because the dispersion of the PGDD exhibits a sharp change there [dashed curve in Fig. 1(b)]. Through nonlinear interaction, such distortions get transferred to the lower-frequency components that are selected by the OBPF to form output pulses. A way to reduce those distortions is to suppress the most distorted spectral components. This can be done by applying a gentle bandpass filtering around the center of each channel [thin solid curve in Fig. 1(b)]. Fortunately, such a bandpass-filtering functionality is inherent to the PGDD: see, e.g., Fig. 3(a) in Ref. 10. Alternatively, one can insert an additional bandpass, spectrally periodic filter after the PGDD to optimize the shape of the amplitude transfer function.

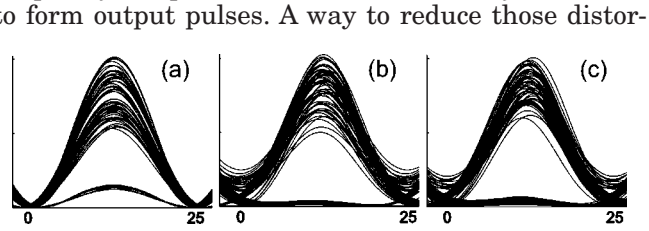

Fig. 3. Optical eye diagrams of the (a) input, as well as of the (b) worst and (c) best channels at the output of the regenerator at 40 Gbits/s. A PGDD is used as the DCM.

To demonstrate the feasibility of the modified multichannel regeneration scheme, we simulated five 400 GHz spaced 40 Gbit/s channels carrying the CSRZ pulses described above. The dispersion coefficients are $D_1=-12$ ps/nm/km and $D_{\mathrm{av}}=-0.2$ ps/nm/km. The 40 GHz OBPF is offset by 80 GHz from the channels' centers. The amplitude response of the PGDD is a periodic 300 GHz wide Gaussian [see Fig. 1(b)]. The average input peak power is 80 mW, and γ_1, L_1, and N are the same as in the 10 Gbit/s simulations. The input pulses have 60% amplitude jitter and an 8 dB extinction ratio [Fig. 3(a)]. Figure 3(b) shows pulses in the worst output channel with the eye-opening improvement over the input of 0.9 dB; the best channel is shown in Fig. 3(c)

In conclusion, we have presented a novel concept of a multichannel all-optical regenerator with a 2R capability. We demonstrated numerically that such a regenerator can improve the signal quality in transmission systems with spectral efficiency up to 0.4 by approximately 1 dB. At 10 Gbits/s this improvement is achieved without additional amplitude filtering by the PGDD, whereas the more spectrally efficient 40 Gbit/s systems do require such filtering.

M. Vasilyev's email address is vasilyev@uta.edu.

References

1. P. V. Mamyshev, in *24th European Conference on Optical Communication* (Institute of Electrical and Electronics Engineers, 1998), Vol. 1, pp. 475-476.
2. Y. Su, G. Raybon, R.-J. Essiambre, and T.-H. Her, IEEE Photonics Technol. Lett. **15**, 350 (2003).
3. N. Yoshikane, I. Morita, and N. Edagawa, Electron. Lett. **38**, 1570 (2002).
4. M. Matsumoto, J. Lightwave Technol. **22**, 1472 (2004).
5. T. Ohara, H. Takara, A. Hirano, K. Mori, and S. Kawanishi, IEEE Photonics Technol. Lett. **15**, 763 (2003).
6. D. F. Grosz, A. Agarwal, S. Banerjee, D. N. Maywar, and A. P. Küng, J. Lightwave Technol. **22**, 423 (2004).
7. X. Wei, X. Liu, C. Xie, and L. F. Mollenauer, Opt. Lett. **28**, 983 (2003).
8. L. F. Mollenauer, A. Grant, X. Liu, X. Wei, C. Xie, and I. Kang, Opt. Lett. **28**, 2043 (2003).
9. C. K. Madsen, G. Lenz, A. J. Bruce, M. A. Cappuzzo, L. T. Gomez, and R. E. Scotti, IEEE Photonics Technol. Lett. **11**, 1623 (1999).
10. C. R. Doerr, L. W. Stulz, S. Chandrasekhar, L. Buhl, and R. Pafchek, in *Optical Fiber Communications Conference (OFC), Postconference Digest*, Vol. 70 of OSA Trends in Optics and Photonics Series (Optical Society of America, 2002), paper PD FA6.
11. T.-H. Her, G. Raybon, and C. Headley, IEEE Photonics Technol. Lett. **16**, 200 (2004).